Glassy behavior and dynamic tweed in defect-free multiferroics

Xiaofei Wang, Ekhard K. H. Salje, Jun Sun, and Xiangdong Ding

Citation: Appl. Phys. Lett. **112**, 012901 (2018); doi: 10.1063/1.5006034
View online: https://doi.org/10.1063/1.5006034
View Table of Contents: http://aip.scitation.org/toc/apl/112/1
Published by the American Institute of Physics

Glassy behavior and dynamic tweed in defect-free multiferroics

Xiaofei Wang,[1] Ekhard K. H. Salje,[1,2,a)] Jun Sun,[1] and Xiangdong Ding[1,a)]
[1]State Key Laboratory for Mechanical Behavior of Materials, Xi'an Jiaotong University, Xi'an 710049, China
[2]Department of Earth Sciences, University of Cambridge, Cambridge CB2 3EQ, United Kingdom

(Received 21 September 2017; accepted 11 November 2017; published online 2 January 2018)

Multiferroics often show significant elastic fluctuations even when the transition is strongly stepwise. Molecular dynamics simulations of a generic toy model show the appearance of tweed nanostructures (cross hatched patterns) in the paraelastic phase just above the transition point. This tweed lowers the elastic modulus C_{12} when approaching the transition temperature. The spatial and temporal correlations of the tweed structure follow the Vogel-Fulcher relationship, and the Vogel-Fulcher temperature is slightly below the transition temperature T_{trans}, preventing this glassy state to freeze completely. Spatial correlations of shear strain show that the size of tweed patches reaches about eight lattice spacings near T_{trans}. Cross- and rod-shaped diffuse scattering, similar to that in relaxors, emerges around {hh0}* and {h00}* Bragg reflections. The viscosity of the sample increases dramatically at the transition point with a significant precursor increase in the tweed regime. *Published by AIP Publishing*. https://doi.org/10.1063/1.5006034

Tweed (cross hatched pattern) is often found as a precursor to ferroic[1] and martensitic phase transitions.[2–7] It was studied extensively[8–10] and related to fluctuations of the ferroelastic order parameters.[11–14] Two approaches have been taken previously to describe the precursor tweed. The first relates the dynamics of tweed to spin-glass dynamics,[14] and the second shows that the precursor tweed is strongly pinned.[15] Our work differs greatly from these approaches because we do not consider ground-state properties[14] but thermal fluctuations in the parent phase. We also avoid defects as agents for stabilizing nanostructures and deal with the dynamics of a defect free matrix. The only sources for tweed formation are the thermal elastic fluctuations of the strain order parameter, which grows when the transition point is approached. We show that such fluctuations are strong even in first order transitions and that the dynamic tweed has all the hallmarks of glass dynamics.

In general, nanoscale fluctuations in the martensitic or ferroelastic phase lead to complex strain patterns such as domain glasses[3,7,16,17] and highly twinned structures in the ferroelastic phase.[7] Previous computer simulations[18–20] showed the formation of a twin pattern is an a-thermal process at low temperatures, which follows the power law or Vogel–Fulcher (VF) statistics at high temperatures. This thermally activated VF behavior is one typical feature of glass dynamics but is also found in materials that are conventionally not described as "glass". Their "glass" dynamics is then intrinsic and does not require extrinsic defects. If extrinsic defects are present, the dynamics of complex strain patterns in martensitic or ferroelastic state is different: the transition can either be suppressed[21–26] or a transformation from fine-scale tweed to a coarser chessboard pattern occurs during spinodal decomposition.[27] For weaker disorder, the ferroic state may contain fluctuations of the order parameter which typically lead to relaxor type behavior.[28,29] Glassy behavior appears also without the contribution of extrinsic defects. For instance, non-Debye relaxations appear in $LaAlO_3$ due to the jamming and pinning of domain walls.[30] Glass-like frequency dispersion was found in $KMn_{1-x}Ca_xF_3$ and attributed to a broad distribution of domain wall lengths and orientations.[31] The elastic moduli of cubic $BaTiO_3$ follow a thermally activated Vogel–Fulcher (or power law) relaxation with $\Delta C \propto \exp[E_a/k_B(T - T_{VF})]$.[32,33] The Vogel–Fulcher temperature, T_{VF}, is slightly below the cubic to tetragonal transition, and the activation energy, E_a, may correspond to the typical hopping energy of intrinsic "defects" such as disordered Ti positions in cubic $BaTiO_3$.[33–36]

About 30 years ago, Sokoloff and collaborators[34] found a central mode (CM) in $BaTiO_3$ as indication of eight-site hopping of Ti. More recently, relaxor-type behavior in $BaTiO_3$ was found with the formation of polar nanoregions (PNRs),[35] which are widely assumed to cause the frequency dispersion of relaxor ferroelectrics[36] and tweeded $LaAlO_3$.[37] It appears that order-disorder systems stabilize tweed strain patterns more effectively than displacive materials. Nevertheless, following Refs. 16 and 38, we show that tweed is indeed expected to be a common feature in displacive ferroelastic systems.

We simulate the glassy behavior of tweed by a well-established model for ferroelastic transitions based on spring-mediated interactions.[18–20,39–42] The potential energy $U(r)$ contains first-nearest atomic interactions $20(r-1)^2$, second-nearest interactions $-10(r-\sqrt{2})^2 + 8000(r-\sqrt{2})^4$, third-nearest interactions $8(r-2)^4$, and forth-nearest interactions $-10(r-\sqrt{5})^2 + 5100(r-\sqrt{5})^4$, where r is the atomic distance. The first-nearest atomic interactions and third-nearest interactions define the elastic background. The second-nearest interactions and forth-nearest interactions define the Landau double-well potential of the ferroelastic phase transition. Specifically, these non-convex interactions reduce the symmetry of the square or cubic unit cell to monoclinic and hence generate a tweed structure and glass-dynamics. We tested the potential for a wide range of parameters that cover a typical elastic behavior of ferroelastic

a)Electronic addresses: ekhard@esc.cam.ac.uk and dingxd@mail.xjtu.edu.cn

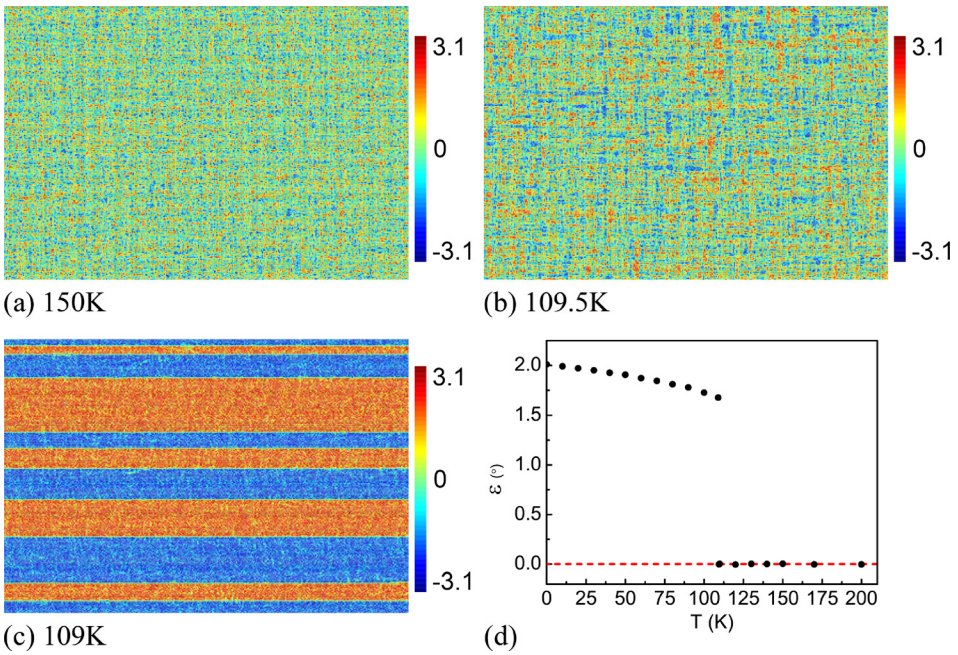

FIG. 1. Atomic configuration at 150 K (a), 109.5 K (b), and 109 K (c). At 109.5 K, the system shows a tweed structure. (d) Temperature evolution of the order parameter.

materials (such as $SrTiO_3$) and found that the tweed formation is a very robust phenomenon. The equilibrated unit cell above T_{trans} and below T_{trans} has the shape of the square and the parallelogram with the shear angle of 2°. The equilibrium lattice constant is $a = 1$ Å and atomic mass $M = 100$ amu with 250 000 (500×500) atoms.[18–20,39–42] Periodic boundary conditions were used to avoid surface effects. We relax the structure between 200 K and 109.5 K for 200–500 ps. Subsequently, another relaxation for 100 ps is performed to collect fluctuation data using isothermal-isobaric ensemble and Berendsen thermostat.[43–45]

The temperature dependences of the atomic configuration and the strain order parameter are shown in Fig. 1. Atoms are colored according to their shear angles, which are defined as $\varepsilon = \varepsilon_{ver} + \varepsilon_{hor}$. ε_{ver} and ε_{hor} measure the local shear angle in the vertical and horizontal directions and are calculated over chains of three atoms.[18–20] At 150 K [Fig. 1(a)], well above the transition point, nanodomains are distributed randomly without tweed. At 109.5 K [Fig. 1(b)], the nanostructure is very different with tweed fairly well displayed with its horizontal and vertical domains. The size of the largest nanodomains reaches a few tens lattice constants.[8] Nano-domains merge and form large stripes at the transition temperature T_{trans} [Fig. 1(c)] to form the typical ferroic twin domain structure. Above $T_{trans} \sim 109$ K, the macroscopic order parameter is zero and changes abruptly at T_{trans} [Fig. 1(d)].

Figure 2(a) shows the slowing-down of the time autocorrelation of the local shear angle $C(t) = \frac{1}{N}\sum_{i=1}^{N} \langle \varepsilon_i(0)\varepsilon_i(t)\rangle$, where N and ε_i are the atom number in the system and the shear angle of atom i, respectively. $<>$ denotes the thermal average. This indicates that before the phase transition, the dynamics of atoms slows down when approaching the transition temperature. This acoustic softening differs from results in multi-atom systems like $0.75PbMg_{1/3}Nb_{2/3}O_3$–$0.25PbTiO_3$ relaxors with typical optical soft modes.[46] In our model, we have no optical soft mode, and all dynamical interactions are related to acoustic or tweed excitations.

We derive the acoustic loss[47] $S''(v) = \frac{\pi}{h}(1 - e^{-hv/k_BT}) \int_{-\infty}^{\infty} C(t)e^{-i2\pi vt}dt$ and $S'(v) = \frac{2}{\pi}\int_0^{\infty} S''(v')\frac{v'}{v'^2 - v^2}dv'$ to calculate the elastic constant C_{12} at zero frequency (where h, k_B, and v are the Planck constant, the Boltzmann constant and the frequency, respectively[47]). This value is then checked against the value determined by direct strain-stress simulations. The agreement is excellent and proves that the slow time relaxation of the correlation function is indeed due to elastic softening. The quantitative temperature evolution of the elastic response beyond the phonon branch was already predicted by Born and Huang.[48] The elastic constant C_{12} follows the power law[49] at $T > T_{trans}$ as $C_{12} = A\ (T - T_{trans})/T_{trans} - \Delta C_{12}$ with $\Delta C_{12} \sim (T - T_{trans})^{-\kappa}$. The predicted exponent κ varies from 0.5 for dimension = 3, via 1 in the two-dimensional case, to 1.5 in dimension = 1.[50,51] Figure 3 shows the good agreement between the analytical shape and simulation results.

We now focus on the temperature evolution of the frequency spectra of the shear strain distribution. As shown in Fig. 4(a), the elastic anomaly appears as central mode (CM) excitation. This excitation shows the typical "slowing down" from 5 THz at 200 K to ca. 0 at 109.5 K when approaching

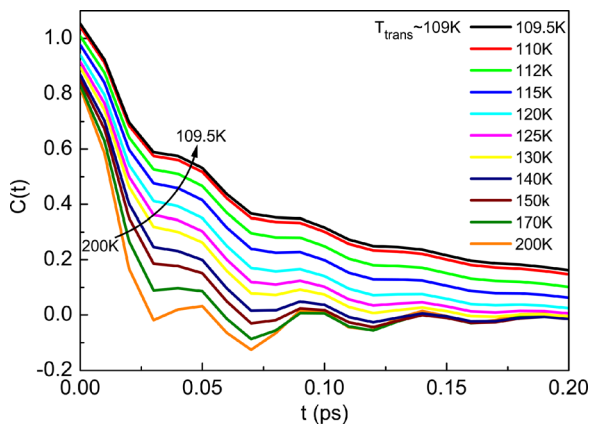

FIG. 2. Time evolution of the time autocorrelation of the local shear angle.

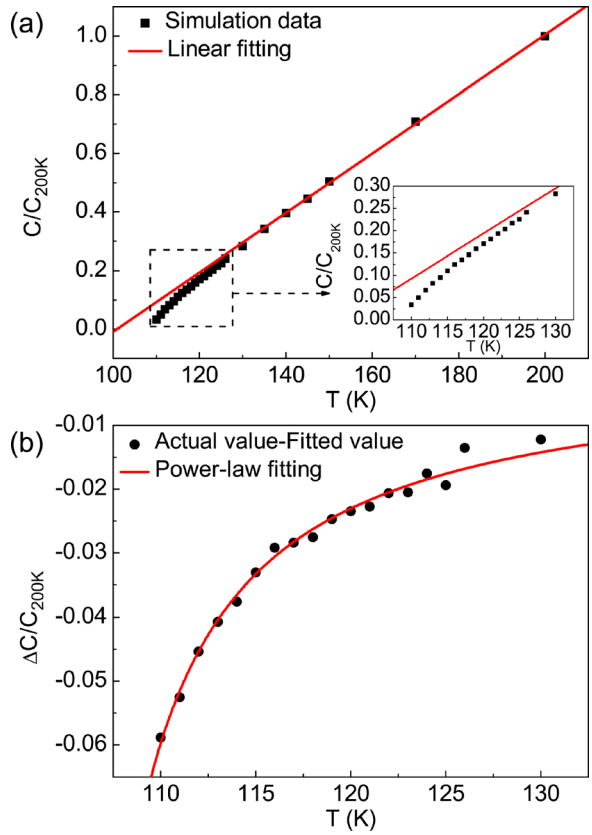

FIG. 3. (a) The softening of elastic constant C_{12} from 200 K to 110 K. The red line is the linear fitting for the 6 highest temperatures. (b) The nanostructure related softening is seen as the deviation between the actual value and the fitted value in (a). The red line is the power-law fitting using $\Delta C/C_{200K} = -D[(T - T_{trans})/T_{trans}]^{-\kappa}$, with $D = 0.0036$, $T_{trans} = 103.6$ K, $\kappa = 1$.

T_{trans}. The peak frequency shows again the decrease from a dynamic excitation to a static deformation. The zero-frequency intersection occurs near $T_{trans} = 109$ K [Fig. 4(b)]. This temperature is well above the extrapolated temperature for the elastic fluctuations of 103.6 K.

Figure 5(a) shows the evolution of the diffuse scattering around the (220)* Bragg reflection with temperature.[52] The typical crosses (or stars) of the tweed structure appear at 125 K. The cross extends in [100]* and [010]* directions according to the geometrical extension of the tweed structure. This is confirmed by the diffuse scattering of (200)* and (020)* with streak along [010]* and [100]* directions [Fig. 5(b)], respectively.

Spatial correlations of atomic shear angles are calculated as $C(r_1, r_2) = \frac{1}{N}\langle\sum_{x,y}\varepsilon(x,y)\varepsilon(x+r_1, y+r_2)\rangle$, and its Fourier transform is the correlation in reciprocal space: $\hat{C}(\mathbf{k}_x, \mathbf{k}_y)$. Tweed shows a correlation in the form of a cross, and so, we show data along the arms of the cross. The lines in Fig. 4(c) show the fit using Voigt distributions. The peaks become narrower when approaching T_{trans}. The correlation length (black circles) in Fig. 4(d) is the inverse of the full width at half maximum (FWHM) of the curves in Fig. 4(c), which increases to over 7 lattice spacings when the temperature approaches T_{trans}. The temperature evolution follows the Vogel-Fulcher law $l = l_0 \exp[E/k_B(T - T_{VF})]$, with l the correlation length. The fitted Vogel-Fulcher temperature T_{VF} is 105.7 K. It is lower than the transition temperature of 109 K, and so, the tweed freezing point cannot be reached.

Figure 4(d) shows that the trend in time correlation mirrors that in space when correlations between atoms become stronger near the transition point, while the system needs more time to accommodate these larger atomic shifts. This is analogous to the relaxation behavior in polymer glass.[53]

The correlation length influences strongly the shear viscosity $\eta = \frac{V}{k_B T}\int_0^\infty \langle P_{xy}(0)P_{xy}(t)\rangle\, dt$, where η, V, T, k_B, and P_{xy} are the shear viscosity, the volume of the simulation cell, the temperature, Boltzmann constant, and the off-diagonal component of the pressure tensor, respectively. The temperature evolution of the viscosity fits the Vogel-Fulcher law $\eta = \eta_0 \exp[E/k_B(T - T_{VF})]$ very well (Fig. 6). This phenomenon is already known from fragile glasses, whereas strong glasses show a typical Arrhenius dependence.[54] It shows that viscosity measurements may be a useful way to investigate subtle transitions in ferroelastic and ferroic materials.

The onset of the fluctuations in the transition regime is clearly visible ca. 20 K above the transition point. The

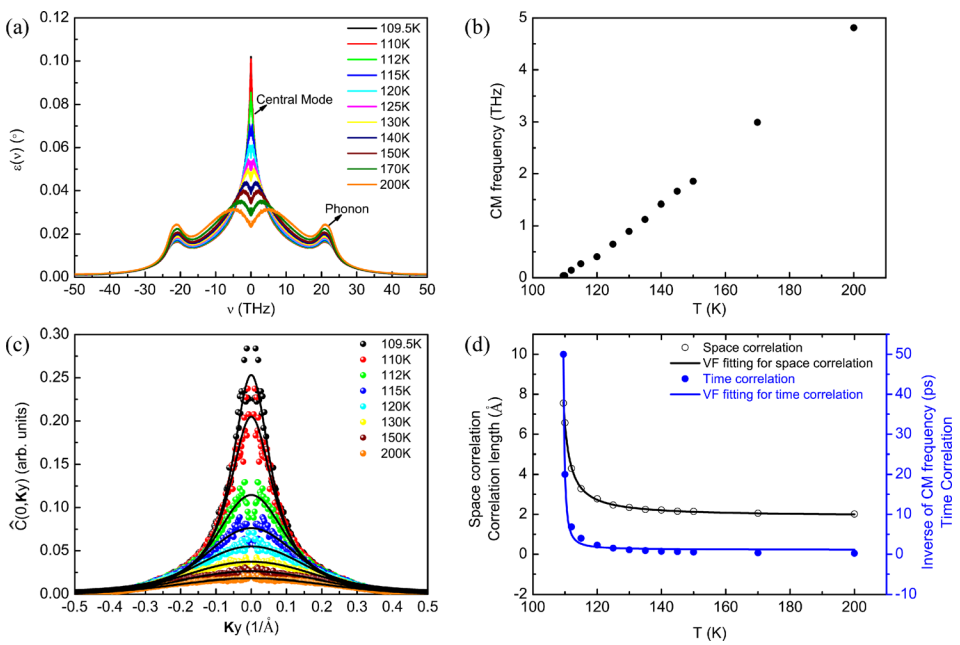

FIG. 4. (a) Fourier transform of the atomic shear angle at variable temperatures. The central mode (CM) tweed peak shifts to lower frequencies when approaching T_{trans}, while the frequency of the phonon peak remains constant. (b) Temperature dependence of the central mode frequency. (c) Space correlation of atomic shear angles in reciprocal space along the y direction. The black lines are the Voigt fittings. (d) Space correlation (black circles) and time correlation (blue dots) evolution with temperature. The black line is the Vogel-Fulcher fitting for space correlation with $T_{VF} = 105.7$ K and $E/k_B = 5.25$ K. The blue line is the Vogel-Fulcher fitting for time correlation with $T_{VF} = 107.8$ K and $E/k_B = 6.44$ K.

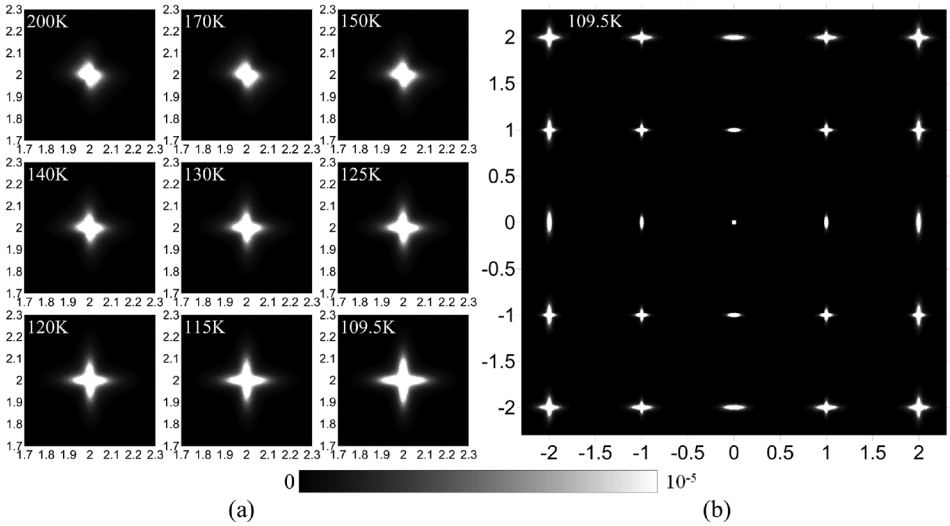

FIG. 5. (a) Simulated diffuse scattering around the $(220)^*$ Bragg reflection. (b) Diffraction pattern along the [001] zone axis at 109.5 K.

fluctuations are highly correlated and lead to the formation of fluctuating geometrical patterns where each "snapshot" reveals a tweed structure. Several physical parameters change in the tweed regime when the transition point is approached, namely, the slowing down of the central peak frequency and its intensity increase. The diffraction patterns change from sharp Bragg reflections to star-shaped crosses. The correlation lengths increase as reflected by the diffuse scattering. Simultaneously, the viscosity of the sample increases and shows a step-wise transition at T_{trans}. All these features are compatible with glass-like behavior as postulated in the concept of "domain glasses" as no extrinsic defects are required to generate this dynamic tweed. Furthermore, in contrast to previous simulations of tweed, we do not introduce components of order/disorder dynamics and show that purely "displacive" ferroelastics and martensites are able to produce tweed, while the central peak frequency converges to zero at the transition point.

The results shed a light on the observation of dynamic tweed in ferroic systems. As an example, we may consider the precursor tweed in $BaTiO_3$ in its cubic phase. While it appears straightforward to relate the tweed to the hopping of Ti between multiple octahedral sites, it appears that such tweed would also appear within a fully displacive picture of the transition. It is now possible to speculate that the hopping component simply enhances the correlations that are seeded by the tweed structure or, alternatively, play a much more important role as driving force for tweed formation. Furthermore, tweed will tend to generate polar patterns by flexoelectricity or bi-linear coupling between order parameters. These different scenarios can now be explored quantitatively by resonant piezoelectric spectroscopy[32] or Brillouin scattering techniques.

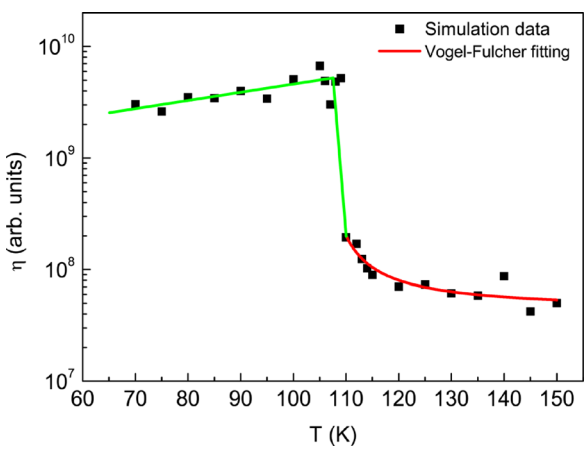

FIG. 6. Temperature dependence of the viscosity. The red line is fitted by the Vogel-Fulcher relation with $\eta_0 = 4.72 \times 10^7$, $T_{VF} = 103.1$ K, and $E/k_B = 10.66$ K. The green line is the guide for the eye.

We appreciate the support of the Natural Science Foundation of China (51320105014, 51621063, and 51231008) and the 111 project (B06025). E.K.H.S. is also grateful to the Engineering and Physical Sciences Research Council (EP/P024904/1) and the Leverhulme Foundation (RPG-2012-564) for support.

[1]E. K. H. Salje, Annu. Rev. Mater. Res. **42**, 265 (2012).
[2]R. Strychor, J. C. Williams, and W. A. Soffa, Metall. Trans. A **19**, 225 (1988).
[3]S. M. Shapiro, B. X. Yang, Y. Noda, L. E. Tanner, and D. Schryvers, Phys. Rev. B **44**, 9301 (1991).
[4]P. C. Clapp, J. Rifkin, J. Kenyon, and L. E. Tanner, Metall. Trans. A **19**, 783 (1988).
[5]D. Schryvers, Philos. Mag. A **68**, 1017 (1993).
[6]N. Resnina, S. Belyaev, A. Shelyakov, V. Rubanik, V. Rubanik, Jr., R. Konopleva, V. Chekanov, E. Ubyivovk, and M. Krzhizhanovskaya, Intermetallics **67**, 69 (2015).
[7]J. Liu, Z. Liu, and X. Jin, Philos. Mag. **94**, 56 (2014).
[8]E. Salje and K. Parlinski, Supercond. Sci. Technol. **4**, 93 (1991).
[9]I. Parsons, J. D. Fitz Gerald, M. T. Heizler, L. L. Heizler, T. Ivanic, and M. R. Lee, Contrib. Mineral. Petrol. **165**, 931 (2013).
[10]E. K. H. Salje, Am. Miner. **100**, 343 (2015).
[11]K. Parlinski, V. Heine, and E. K. H. Salje, J. Phys. Condens. Matter **5**, 497 (1993).
[12]A. M. Bratkovsky, S. C. Marais, V. Heine, and E. K. H. Salje, J. Phys. Condens. Matter **6**, 3679 (1994).
[13]Y. M. Jin, A. Artemev, and A. G. Khachaturyan, Acta Mater. **49**, 2309 (2001).
[14]S. Kartha, T. Castán, J. A. Krumhansl, and J. P. Sethna, Phys. Rev. Lett. **67**, 3630 (1991).
[15]X. Ren, Y. Wang, Y. Zhou, Z. Zhang, D. Wang, G. Fan, K. Otsuka, T. Suzuki, Y. Ji, J. Zhang, Y. Tian, S. Hou, and X. Ding, Philos. Mag. **90**, 141 (2010).
[16]E. K. H. Salje, X. Ding, and O. Aktas, Phys. Status Solidi B **251**, 2061 (2014).
[17]E. K. H. Salje, X. Ding, Z. Zhao, and T. Lookman, Appl. Phys. Lett. **100**, 222905 (2012).

[18]E. K. H. Salje, X. Ding, Z. Zhao, T. Lookman, and A. Saxena, Phys. Rev. B **83**, 104109 (2011).
[19]X. Ding, T. Lookman, Z. Zhao, A. Saxena, J. Sun, and E. K. H. Salje, Phys. Rev. B **87**, 094109 (2013).
[20]X. Ding, Z. Zhao, T. Lookman, A. Saxena, and E. K. H. Salje, Adv. Mater. **24**, 5385 (2012).
[21]S. Sarkar, X. Ren, and K. Otsuka, Phys. Rev. Lett. **95**, 205702 (2005).
[22]Y. Ji, X. Ding, T. Lookman, K. Otsuka, and X. Ren, Phys. Rev. B **87**, 104110 (2013).
[23]X. Ren and K. Otsuka, Phys. Rev. Lett. **85**, 1016 (2000).
[24]X. Ren, Y. Wang, K. Otsuka, P. Lloveras, T. Castán, M. Porta, A. Planes, and A. Saxena, MRS Bull. **34**, 838 (2009).
[25]Y. Zhou, D. Xue, Y. Tian, X. Ding, S. Guo, K. Otsuka, J. Sun, and X. Ren, Phys. Rev. Lett. **112**, 025701 (2014).
[26]J. Zhang, D. Xue, X. Cai, X. Ding, X. Ren, and J. Sun, Acta Mater. **120**, 130 (2016).
[27]Y. Ni and A. G. Khachaturyan, Nat. Mater. **8**, 410 (2009).
[28]P. M. Gehring, S. Wakimoto, Z.-G. Ye, and G. Shirane, Phys. Rev. Lett. **87**, 277601 (2001).
[29]V. Bobnar, Z. Kutnjak, R. Pirc, R. Blinc, and A. Levstik, Phys. Rev. Lett. **84**, 5892 (2000).
[30]R. J. Harrison, S. A. T. Redfern, and E. K. H. Salje, Phys. Rev. B **69**, 144101 (2004).
[31]W. Schranz, P. Sondergeld, A. V. Kityk, and E. K. H. Salje, Phys. Rev. B **80**, 094110 (2009).
[32]O. Aktas, M. A. Carpenter, and E. K. H. Salje, Appl. Phys. Lett. **103**, 142902 (2013).
[33]E. K. H. Salje, M. A. Carpenter, G. F. Nataf, G. Picht, K. Webber, J. Weerasinghe, S. Lisenkov, and L. Bellaiche, Phys. Rev. B **87**, 014106 (2013).
[34]J. P. Sokoloff, L. L. Chase, and D. Rytz, Phys. Rev. B **38**, 597 (1988).
[35]E. Dul'kin, J. Petzelt, S. Kamba, E. Mojaev, and M. Roth, Appl. Phys. Lett. **97**, 032903 (2010).
[36]J. Hlinka, T. Ostapchuk, D. Nuzhnyy, J. Petzelt, P. Kuzel, C. Kadlec, P. Vanek, I. Ponomareva, and L. Bellaiche, Phys. Rev. Lett. **101**, 167402 (2008).
[37]E. K. H. Salje, M. Alexe, S. Kustov, M. C. Weber, J. Schiemer, G. F. Nataf, and J. Kreisel, Sci. Rep. **6**, 27193 (2016).
[38]E. K. H. Salje and M. A. Carpenter, Phys. Status Solidi B **252**, 2639 (2015).
[39]Z. Zhao, X. Ding, T. Lookman, J. Sun, and E. K. H. Salje, Adv. Mater. **25**, 3244 (2013).
[40]E. K. H. Salje, X. Ding, and Z. Zhao, Appl. Phys. Lett. **102**, 152909 (2013).
[41]E. K. H. Salje, X. Wang, X. Ding, and J. Sun, Phys. Rev. B **90**, 064103 (2014).
[42]Z. Zhao, X. Ding, J. Sun, and E. K. H. Salje, J. Phys.: Condens. Matter **26**, 142201 (2014).
[43]H. J. C. Berendsen, J. P. M. Postma, W. F. van Gunsteren, A. DiNola, and J. R. Haak, J. Chem. Phys. **81**, 3684 (1984).
[44]S. Plimpton, J. Comput. Phys. **117**, 1 (1995).
[45]J. Li, Modell. Simul. Mater. Sci. Eng. **11**, 173 (2003).
[46]I. Grinberg, Y.-H. Shin, and A. M. Rappe, Phys. Rev. Lett. **103**, 197601 (2009).
[47]J. P. Sethna, *Statistical Mechanics Entropy, Order Parameters, and Complexity* (Oxford University Press, USA, 2011).
[48]M. Born and K. Huang, *Dynamical Theory of Crystal Lattices* (Oxford University Press, Oxford, 1954).
[49]M. A. Carpenter and E. K. H. Salje, Eur. J. Miner. **10**, 693 (1998).
[50]E. K. H. Salje, M. Zhang, and H. Zhang, J. Phys. Condens. Matter **21**, 335402 (2009).
[51]E. K. H. Salje and H. Zhang, J. Phys. Condens. Matter **21**, 035901 (2009).
[52]C. S. Becquart, P. C. Clapp, and J. A. Rifkin, Phys. Rev. B **48**, 6 (1993).
[53]R. D. Priestley, C. J. Ellison, L. J. Broadbelt, and J. M. Torkelson, Science **309**, 456 (2005).
[54]L. Berthier and G. Biroli, Rev. Mod. Phys. **83**, 587 (2011).